CONFIGURATION OF MODULAR SCAFFOLDS FOR CRANIOMAXILLOFACIAL REGENERATION: A COMPUTATIONAL APPROACH

by

ISABELLA HARKER

A THESIS

Presented to the Department of Computer Science
and the Robert D. Clark Honors College
in partial fulfillment of the requirements for the degree of
Bachelor of Science

May 2025

An Abstract of the Thesis of

Isabella Harker for the degree of Bachelor of Science
in the Department of Computer Science to be taken May 2025

Title: Configuration of Modular Scaffolds for Craniomaxillofacial Regeneration: A Computational Approach

Approved: *Robert Guldberg, Ph.D*
Primary Thesis Advisor

Craniomaxillofacial trauma is an important focus in bone regeneration research due to its relative complexity and importance compared to the larger bones in the body, and due to the high rates of incidence in both military and civilian personnel in battlefield scenarios. This thesis builds off previous work in 3D bio-printing and the development of a modular scaffolding system for craniomaxillofacial regeneration and presents a computational shape fitting model for use with these technologies in a clinical setting. Presented is an evolutionary model which initializes then optimizes a shape fit configuration for a given shape. Testing on simple shapes, a rat skull, and a human mandible sample demonstrates that the model can generate an accurate, stable shape fit configuration in <2 seconds with $>95\%$ connectivity for a variety of shapes with differing sizes and complexities and can be adapted to fit any desired physical block size for the shape fit configuration. This model demonstrates proof of concept for the automated configuration of our modular scaffolding system, which is an important step in future clinical application of this technology.

Acknowledgements

I want to thank my family and friends for all their support and encouragement throughout this process. I also want to thank Ethan Dinh, Angela Lin, and everyone else in the lab for helping me become part of this project and giving me the opportunity to learn. Finally, thank you to Genny and Bob for your mentorship and perspective on this project. It was a wonderful learning experience for me and I hope the insight can inform the future work on the project.

Table of Contents

List of Figures

Introduction

Over the past 2 decades, the incidence of craniomaxillofacial trauma on battlefields has increased substantially, and currently contributes to 40% of casualties (Neubauer et al., 2022). For one example, during Operation Iraqi Freedom between May and September 2005, 61% of all surviving patients acquired head and neck wounds, which constitutes an alarmingly high incidence rate (Lopez & Arnholt, 2007). Additionally, data from facial fractures in Afghanistan suggested that the most common injuries were mandibular, followed by maxillary/zygomatic fractures (Brennan, 2006). Collectively, these bones constitute the major bones of the face. Trauma to this region can be life threatening as well as life altering by disfiguring facial features and impacting the ability of a patient to breathe, eat and drink, ultimately impacting patients' quality of life.

It has been demonstrated that access to in-theater treatments and protocols contributes to higher survival and successful recovery rates of soldiers (Brennan, 2006). Therefore, technologies that can be deployed for in-theater craniomaxillofacial regenerative procedures in frontline hospitals and forward surgical teams, deployed to care for personnel injured in conflict, are likely to see significant positive impact (Valdiri et al., 2015). However, the current standard of care is limited by accessible technologies and often sees limited regenerative strategies in areas without access to such systems. Therefore, it is of interest to patient care to develop easily deployable and customizable regenerative solutions for craniomaxillofacial regeneration.

While there has been significant advance in the field of three-dimensional (3D) bioprinting for bone regeneration, there is a disconnect between the success of this technology in an experimental setting and use in a clinical environment. Modular scaffolding, as opposed to creating custom implants for every patient, are one way to bridge the gap from bench to bedside by increasing ease-of-use and access to regenerative technologies. However, optimization of modular components for complex craniofacial trauma is a relatively unexplored field and requires development of new approaches from both an engineering and clinical perspective. We recently developed a method to 3D-print prefabricated bone regenerative materials in cubes that can be assembled into complex geometries in 3D (Subbiah et al., 2020). Our current technical limitation is creating a model for shape fitting and configuration planning for patient specific craniomaxillofacial defects with complex geometries.

The objective of this project is to create a computational model to optimize the configuration of the modular 3D scaffolding system designed by our collaborators at Oregon Health and Science University (OHSU), as described in Subbiah, et al., 2020. This is a crucial contribution to the overall goal of developing a pipeline to start from a CT-scan of a craniofacial defect and construct an accurate, custom scaffold from prefabricated components in order to aid healing and recovery for patients. Ultimately, completion of this work will help to move this project forward towards translation into a clinical setting with the ability to be deployed in situations such as battlefield wound care.

Background

Craniomaxillofacial surgery and reconstruction faces unique challenges due to the mechanical requirements of the bones and high level of patient-specific variation in form compared to other bones in the body. At this point in time, majority reconstruction of craniofacial bone tissue following a traumatic event relies on either transplant of bone from a distant site such as the tibia, or reconstruction using bone grafting materials and biologic therapies which have minimal form or structure and are stabilized with hand bent metal meshes. Both of these techniques are difficult to deploy in frontline surgical settings, so treatment is limited despite the high prevalence of facial trauma in warzones for both military and civilian personnel (Neubauer et al., 2022).

In recent years, 3D printing has emerged as a transformative technology for the fabrication of enhanced scaffolds for regenerative surgeries (Bertassoni, 2022; Willson & Atala, 2022). 3D printing offers the ability to create custom, defect-matching scaffolds designed to improve host tissue ingrowth and regeneration. However, widespread deployment of 3D bio-printers (3D printers which have been modified to print biologically compatible material) remains distant. In warzones, the need for specialized equipment and personnel to operate 3D bio-printers makes the technology presently incompatible. Given the rates of craniofacial trauma and the typical severity of the injuries, incorporation of a new technology which avoids the need for on-site 3D bio-printers would likely see significant impact on healing and surgery success rates for patients.

There are a number of 3D bioprinting methods which have been shown to accelerate healing in *in-vitro* models, drawing on research in cell growth and substances (S. S. Lee et al., 2023; Subbiah et al., 2023; Thrivikraman et al., 2019). Researchers have had success using 3D bioprinting for dermal wounds on mice, as well as filling osteochronal defects in a theoretical model (Murphy et al., 2020; Willson & Atala, 2022). 3D bio-printing has also been researched as a replacement for metal grafts in bone defect surgeries due to the ability to use materials such beta-tricalcium phosphate (β-TCP) which has similar composition and mechanical properties to bone and allows a high degree of control over the exterior and interior structure of the print, known as a scaffold. Research into optimized scaffold designs and pore structures has shown the ability to achieve high anatomic fidelity in scaffolds while still maintaining control over interior pore structures and improving healing outcomes in both *in vitro* and *in vivo* models (Ho et al., 2022; Pilipchuk et al., 2016; Zopf et al., 2014). This research shows that 3D printing applications to bone reconstruction has the potential to improve healing outcomes for some of the most complicated injuries, including soft-tissue craniofacial reconstruction (Zopf et al., 2014). However, the translation to clinical use has proven difficult due to the scale, cost, and high degree of automation and sterilization required for in situ printing (Willson & Atala, 2022).

As an alternate approach, a joint team from the OHSU and the Phil and Penny Knight Campus for Accelerating Scientific Impact at the University of Oregon, has developed a new scaffold assembly system that uses prefabricated β-TCP scaffolds in the form of rigid, hollow, and stackable microcage modules, resembling LEGO® blocks (Subbiah et al., 2020). These scaffolds have been shown to enhance host tissue invasion and vascularization, as well as closely mimic the compressive strength of mandibular bone (Subbiah et al., 2020). These modular, prefabricated scaffolds retain the benefits of on-demand 3D printing, such as bio-compatible material and custom geometry, without the need for on-site equipment. The proposed modular scaffolds are intuitive, scalable, and capable of being sterilized and pre-packaged for deployment.

Some of the biggest challenges facing 3D bioprinting are the scale of the print job, cost, and availability (Willson & Atala, 2022). Our 3D printed cube system would circumvent these issues and provide a scalable, accessible system for building custom implantable constructs. Additionally, the cubes can be sterilized and prepacked in varying size conformations which can be assembled during surgery to best fit the patients' needs. A similar modular scaffolding strategy has been employed in other systems including with biological materials and titanium (S. S. Lee et al., 2023). However, none of these systems have yet made the leap to automated design of scaffold configuration, therefore, creating a system capable of determining optimal configuration and alignment for a defect will be instrumental for future research in this technology. Additionally, automation of the scaffold configuration process helps in translation by lowering the technical expertise required to utilize the technology. The purpose of using scaffolds and modular systems is to improve healing and surgical outcomes for patients as well as simplify the custom implant workflow for surgeons. While assembly will still be a factor, we aim to minimize complexity to the greatest degree possible.

From a computational perspective, this project involves questions from fields such as geometry, computer graphics, and image processing, and previous work in building LEGO® configurations. Beginning with the latter, using oriented blocks to build a particular shape is a problem that has ultimately defined the LEGO® company, since construction of complex objects from simple blocks is the premise of their enterprise. Over the years, researchers have studied this problem by creating algorithms such as those outlined in *Finding an Optimal LEGO® Brick Layout of Voxelized 3D Object Using a Genetic Algorithm* (S. Lee et al., 2015).

Other similarities between optimizing LEGO® configurations and generating scaffold configurations arise in examining the biomechanical properties that the proposed system must imitate. These include self-supporting assemblies and stable layouts, as well as determining if a particular configuration can hold up to force in various directions. Researchers have developed methods to generate and test layout designs as well as to provide assembly instructions (Testuz et al. (2013), Kim et al. (2014)). Additionally, research by Waßmann and Weicker (2012) proposed a method for judging the stability of a generated sculpture. Our approach will build upon foundational literature in model design and testing and will be adapted to our clinical scenario of complex craniomaxillofacial regeneration.

Beyond shape fit optimization, computational and graphic design constraints must be addressed for computationally demanding workflows. There are a variety of analysis methods used in computer graphics to address stability and friction for model simulation (Smith et al., 2012; Umetani et al., 2012). Layout optimization theory can also be applied to design problems such as 3D fabrication (Prévost et al., 2013; Stava et al., 2012) and furniture design (Umetani et al., 2012). The main difference in methodology and use lies in the discrete nature of tiling configurations such as LEGO® or our modular scaffolding system where orientations, sizes, and locations of blocks are allowed far less flexibility in contrast to a field like furniture design.

Optimized shape fitting and tiling intersects with other fields such as differential geometry and computer graphics. Handling voxelization and data structures for representations of 3D objects is one of the defining problems in computer modeling and graphics over the last few decades. The theory of ray tracing and rasterization algorithms is deeply studied and can provide insight into our problem of configuration. The premise of this work will be to apply previously developed shape fitting algorithms to our specific use case to achieve the desired surgical planning required by the end users, here defined as surgeons.

Overall, this project combines the existing literature on theoretical computational shape modeling with new advances in biomechanical and regenerative technologies. Therefore, our aim is to merge and adapt previous research to the specific use context of craniomaxillofacial regeneration and create a new computational model that will help to improve patient care.

Methods

Evaluation Metrics

Shape fit configuration refers to the arrangement of blocks used to build a structure. Shape fit configurations will be evaluated on three primary metrics: (1) number of blocks used,

(2) the overall connectivity or fill score of the configuration and (3) distribution of block shape and size. All three of these metrics relate directly to the clinical application of this technology because a successful configuration must be both structurally sound and easy to assemble on-site, with a bonus if a smaller distribution of blocks sizes is required.

The metrics concerning the blocks, both number and dimensions, are a proxy for ease of assembly. To this end, we will be prioritizing larger blocks and configurations which use the smallest number of overall blocks. Our estimate of a reasonable number of blocks for a shape fit configuration is 50, which is the numerical benchmark used for evaluating shape fit configurations in testing. The connectivity or fill score relates to the graph representation of the shape fit configuration, where edges represent a connection between two blocks. This percentage score represents the percentage of blocks which are connected each other in the final structure, where a score of 100% means complete connection. In general, maximizing this score is one of the primary goals of the model to consistently generate stable configurations.

The future work of this project will involve evaluating the shape fit configurations using finite-element modeling and biomechanical simulation to determine how closely they match the properties found in native bone. While this is not an immediate concern as the biomechanical properties of the blocks themselves are not fully actualized, it is a significant component of the project given the eventual clinical applications.

Further discussion with clinicians will allow for translational evaluation of the utility of the proposed system. While it is likely that certain evaluation criteria cannot be entirely determined before testing, especially the biomechanical criteria and ease-of-use for the end user, those concerns lie out of scope for this research project.

Model Development

The computer model is an evolutionary algorithm which follows conceptually from previous research by Lee et al. (2015) and Luo, et al. (2015). Once a CT-scan or comparable shape has been pre-processed to provide a binary representation of the structure, it can be scaled and run through the generative algorithm to create a shape fit configuration.

During the building process, the model operates in a bottom-up manner, where each layer is built on top of the previous layer with the goal of optimizing connectivity of the whole structure from the beginning. This allows for efficient backtracking as well as the ability to pinpoint the weaker layer connections throughout the process. The layers which do not meet connectivity requirements can then be re-evaluated to determine whether the model can be improved at those points.

Preliminary Testing

Following initial model development, we will test the shape fit configuration for accuracy, biomechanical stability, and optimization ability using a set of preliminary artificially constructed data alongside experimental data, which consists of several deidentified craniofacial CT-scan samples. These tests will allow us to revise the models as necessary so that they meet the defined criteria and produce an optimized shape fit configuration for a wide range of inputs.

The test data set consists of two simple shapes, a torus and a cube, along with a simplified rat skull segment from a CT-scan. These tests demonstrate the ability of the model to compute shape fit configurations for non-rectangular geometries and shapes with holes or other non-regular features. Since the eventual goal is to use this system to improve patient care for craniomaxillofacial defects, which are often irregular in shape, this is a crucial step in algorithm design and ensuring the robustness of the model.

Experimental Testing

To validate the proposed shape fitting algorithm, we will utilize the patient CT-scans to generate a defect shape (volume) which can be used to confine and test the model. CT-scans will be analyzed for the defect region in a slice-by-slice format to reconstruct the defect region in a 3D volume. We will then generate a cube configuration for the volume using the generated shape fitting models. This is an important pre-clinical validation step for our model.

Modeling

In a 3D shape fit configuration, all blocks are of height 1 unit with varying length and width, with the smallest block having dimensions 1x1x1 (height x width x length) up to a maximum size of 1x5x5. The units are defined by the user so that 1 unit is equivalent to the desired physical size of a 1x1x1 block. This was done to simplify the problem computationally and avoid floating point errors during computation by using integer scaling for the virtual blocks. It also allows for a range of physical block dimensions to be tested by physically scaling the initial shape differently.

The shape fit configuration is represented by a directed graph during generation and optimization, with individual blocks as vertices and block connections as directed edges from a lower layer to a higher layer. Figure 1 shows this breakdown on a two-dimensional (2D) example, with blocks of height 1 unit and length up to 4 units. The graph representation was chosen because it provides straightforward support for the analytical tools used in optimization, specifically and primarily a depth-first search algorithm. The model takes advantage of the graph structure both to optimize inter-layer connectivity and to ensure the final shape fit configuration forms a connected whole.

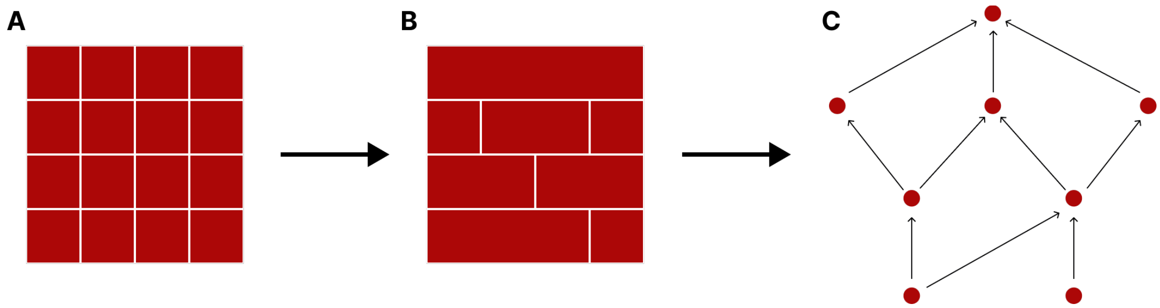

Figure 1. (A) A sample 2D square for allocation. (B) A shape configuration for the grid (layers are horizontal, connections between blocks are vertical overlaps). (C) The shape configuration represented as a directed graph with nodes representing blocks and edges representing block connections.

For a given shape problem, the pre-processing step results in a 3D binary array, with a value of 1 indicating a filled space and a value of 0 indicating empty space. Once the shape has been formatted correctly, the shape is scaled based on the initial resolution so that the unit size of the array matches the desired block dimensions, returning a new, smaller 3D binary array representing the scaled shape. This step is necessary because CT-scan resolution, typically <1mm, does not match the projected block size of 4-10mm. Once the image has been scaled to a proper resolution, the configuration algorithm operates on the resulting array.

The shape fit configuration is built from the bottom layer up, which allows each individual layer to be optimized before the next is considered. For each layer, an initial block cover is generated using a greedy random selection method by selecting a fill voxel randomly, fitting the largest block by area to that voxel, then repeating until the entire layer is filled. The term greedy refers to the fact that it will choose the optimal choice for a certain time step, i.e. the largest block, regardless of whether this block choice is optimal for the final configuration. This improves initial connectivity compared to a procedural allocation because boundaries between blocks are randomized so the number of connections between blocks is increased instead of two blocks in consecutive layers only have a single edge to the block directly above or below them.

Following the initial random fill step, the model follows an evolutionary process which chooses one block to split into 1x1 blocks and one block to merge with its neighbors at each step, shown in Figure 2. The block split step allows the model to try different configurations and orientations of blocks to improve the connectivity, while the merge step eliminates the smallest blocks from the configuration. This evolution is run for a maximum of $n=30$ generations or until an optimal allocation is found. The loop limit exists to avoid the model getting stuck in an infinite loop in the case that the shape is unsolvable for any reason.

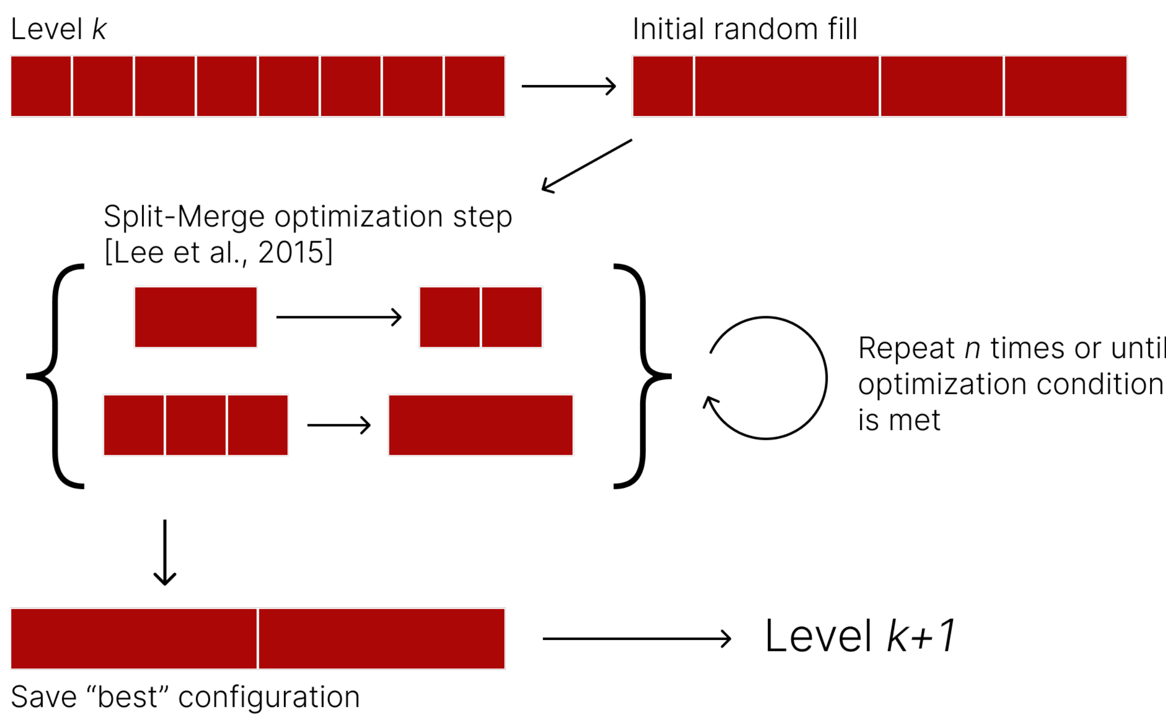

Figure 2. Steps of the evolutionary model for generating level k.

The final step after the evolutionary process is eliminating as many 1x1x1 blocks as possible by merging them with their neighbors. This step is done for two reasons. First, it improves connectivity because 1x1x1 blocks cannot contribute to overall connection as well as larger blocks because their only connections are vertical, and connectivity is overall a horizontal measurement. Second, it decreases the overall number of blocks that are used in the configuration by reversing any uncorrected splitting and accounting for 1x1 blocks which may have been missed by the optimization step.

From an abstract standpoint, if every two layers have complete connection, then the whole shape must also be completely connected. Although this is not always achievable depending on the shape, it is still the case that coming as close as possible to optimal configuration for every consecutive pair of layers will ensure stability across the final structure.

We rate a configuration based largely on the connectivity or fill score, which is the percentage of blocks in the final configuration which belong to the major connected subgraph. In certain cases, not every block is connected to the rest of the configuration. This can be due to the arrangement of blocks or the initial structure of the shape itself, as particularly narrow segments or thin features can inhibit block placement. We do not require every configuration to consist of only one connected structure, but rather take as the final configuration the largest connected shape within the configuration by volume. The current benchmark for connectivity is a score of >95%, which indicates that 95% of the initial shape is represented by the shape fit configuration. However, this benchmark may be subject to change in the future.

The connectivity score combined with the number of blocks allows for analysis of the shape itself as well as the model performance and gives some insight on whether the physical block size is appropriate for the initial shape.

Preliminary Results

Initial tests were run on a 3x3x3 cube and an 3x8x8 torus, shown in Figure 3. The cube was chosen as the simplest relevant testing case to expose any bugs in the model, and the torus was chosen to test some initial edge cases like holes and less structured corners.

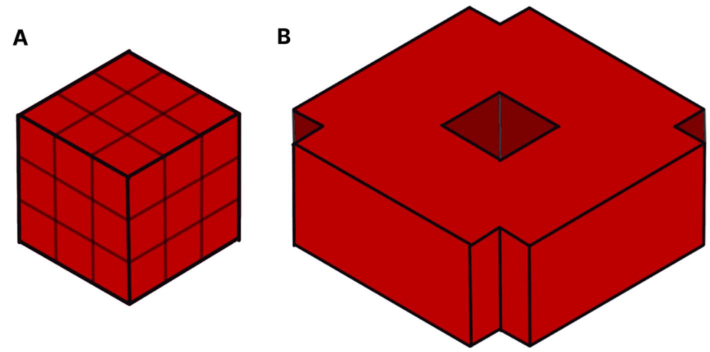

Figure 3. (A) The 3x3x3 test cube. (B) The 3x8x8 test torus.

The block distribution for both shapes trends towards longer and skinnier blocks instead of square blocks, but importantly the count of 1x1x1 blocks is limited as desired due to the final model merge step. On the torus, the model was able to generate completely connected configurations in 0.12 ± 0.07 seconds across 100 trials, and the generation for the cube was equally fast. Figure 4 (below) shows the distribution of blocks for configurations of the torus across 100 trials. Longer, skinnier blocks are more common than the square blocks, and the 1x1x1 blocks are not majorly dominating the block distribution. The model's preference for less square blocks is consistent across trials, as experimental data also demonstrates.

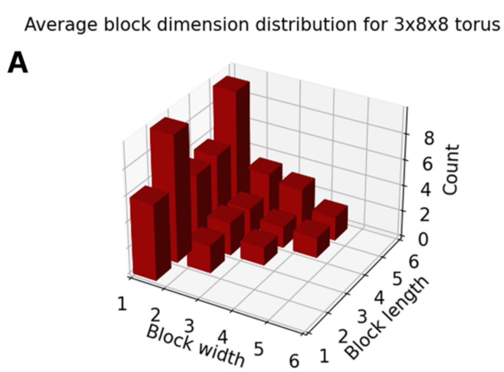

B

BlockX (width)	BlockY (length)	Count (mean)	Count (std)
1	1	5.89	2.204064427
1	2	9.81	3.276263115
1	3	5.52	2.43918019
1	4	5.75	1.807622748
1	5	9.51	2.920599254
2	2	2.148148148	1.177055451
2	3	2.549450549	1.368914997
2	4	2.288888889	1.107995632
2	5	3.747474747	1.565689149
3	3	1.396825397	0.578440227
3	4	1.652777778	0.884428915
3	5	3.298969072	1.355895477
4	4	1.59375	0.842591798
4	5	1.853658537	0.813333268

Figure 4. (A) Histogram showing distribution of block dimensions across 100 generated configurations for the 3x8x8 torus. (B) Table containing data for the histogram.

Prior to the experimental test on human mandibular data, we also tested the workflow and model on a CT-scan of a rat skull. The rat skull was chosen both because it originated from CT-scan data and because it is a cranial bone scan, so it can act as a good proxy for the intended use case. For this trial, only the 4mm block size was considered because the larger blocks were unable to accurately represent the rat skull segment due to its small initial size. The 4mm blocks, while still somewhat large, were able to capture the important details of the shape. The most significant metric of the complexity configuration is the block count, especially considering potential clinical applications. Using the 4mm blocks, the shape fit configurations for the rat skull used 12.44 ± 0.62 blocks, which is well below our set threshold of 50 blocks.

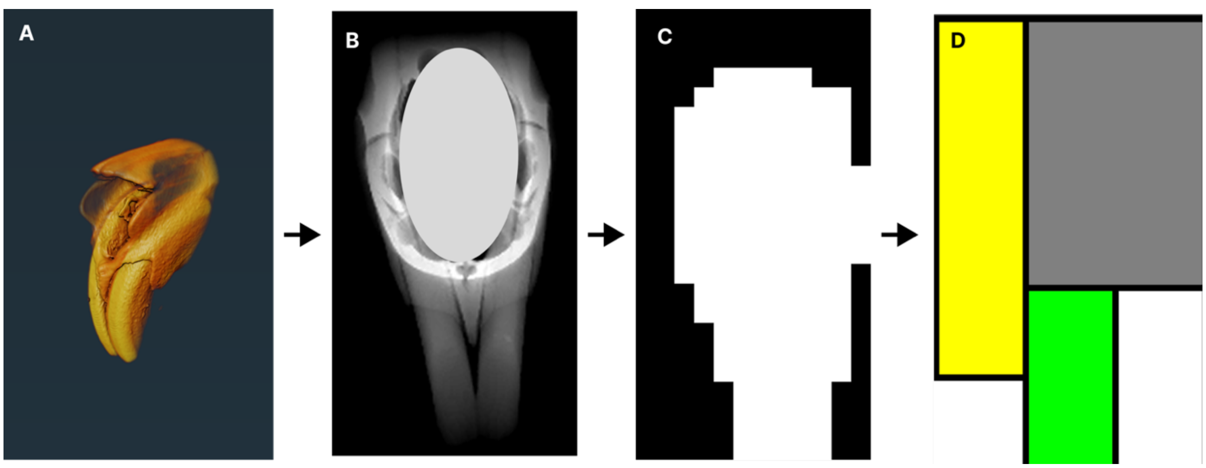

Figure 5. (A) 3D image of selected segment of rat skull. Initial scale was 78 (B) Average Z-projection of rat skull segment. The grey oval indicates to-be-filled space to make the object completely solid. (C) One slice of the rat skull scan following processing, including filling in the holes to align the scan with our expectation of solid shapes. (D) The same slice of the rat skull with the block configuration shown using 4mm blocks.

Despite the increased complexity of the rat skull shape compared to the two test objects, the cube and the torus, the model was able to generate well-connected shape fit configurations. The model finished in 0.17 ± 0.01 seconds across 100 randomized trials and the generated configurations had an average connectivity score of 95.7% ± 4.90%. Note that due to the low resolution of the block size for this particular test, a connectivity score of 95% indicates that only one block was disconnected from the final configuration, rather than a symptom of a larger error in the model.

Overall, the preliminary results show that the model's ability to generate a well-connected configuration within a reasonable timeframe on both trivial (cube, torus) and non-trivial (rat skull) shapes.

Experimental Results

We obtained de-identified human cranial CT-data for experimental testing (J Wallner & J Egger, 2018; Wallner et al., 2018). From the initial scans, we segmented the mandible using the Mimics software suite then processed the resulting image using the workflow that was previously established with the rat CT-scan, as shown in Figure 6. In addition to testing the model on the full mandible, we created and tested a mandibular segment consisting of a 45mm sagittal cut of the ramus on the right side of the mandible to determine whether there was a significant difference in performance between the two scenarios. We experimented with three potential block sizes (4mm, 7mm, 10mm) with the goal of generating a shape which mimics the original bone structure as closely as possible while requiring a reasonable number of blocks to assemble, which is our benchmark of <50 blocks.

The tests with the full mandible show that the 4mm blocks are far too small, with the configurations requiring 251 ± 36 blocks for building across 100 trials. The shape fit configurations with the 7mm blocks required 93 ± 16 blocks, which is still higher than our benchmark but shows significant improvement over the 4mm blocks. The largest block size that we tested, 10mm, was able to just meet the benchmark on average, requiring 50 ± 7 blocks for the shape fit configurations. The tests with the mandibular segment, on the other hand, showed much more realistic block counts for all the block sizes, with the 4mm configurations requiring

78 ± 19 blocks and both the 7mm and 10mm block configurations falling below the 50-block threshold, at 28 ± 7 blocks and 18 ± 3 blocks respectively.

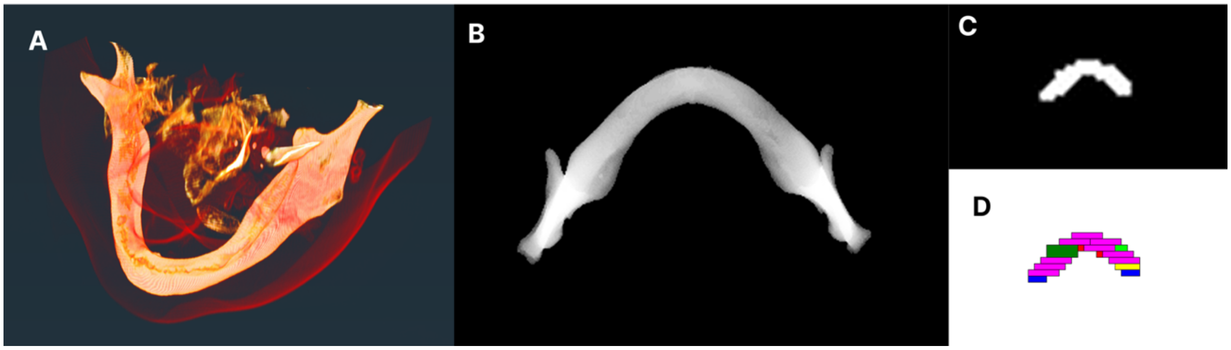

Figure 6. (A) 3D view of the mandible from the initial CT scan. (B) An average z-projection view of the mandible, top-down. (C) One slice of the mandible following the pre-processing step and scaled to 4mm/pixel. (D) The same z-slice of the shape with the model output overlaid.

The model saw an overall drop in performance with the mandible tests compared to the previous examples. For the 7mm blocks, the time to build the configuration increased, likely due to both its size and complex shape, to 1.60 ± 0.06 seconds across 100 trials. Additionally, several of the configurations scored <70% on connectivity, suggesting that the model only connected one half of the mandible and was not able to unify the two sides.

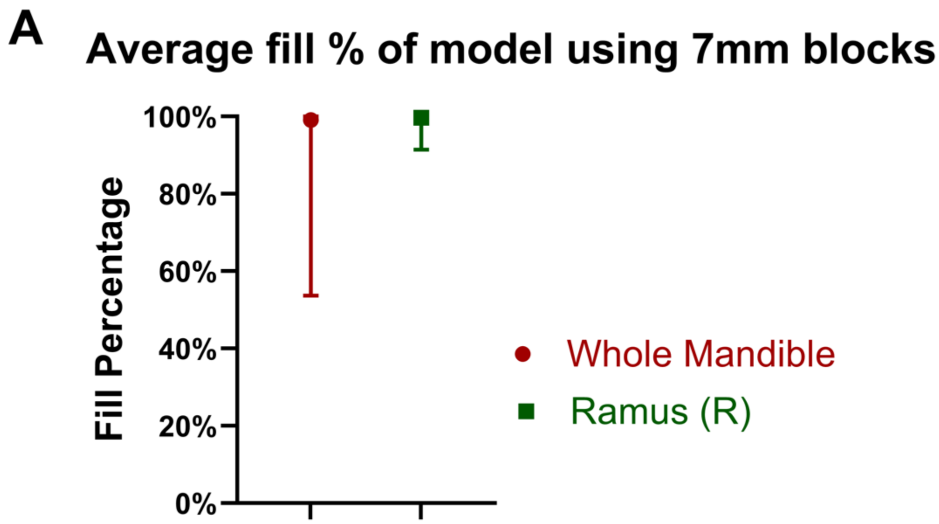

Figure 7. (A) Average fill % of the model across 100 trial runs for the whole mandible and the 45mm sagittal cut of the right ramus. Displayed is mean and range of the data. Both images were scaled to 7mm/pixel, which was the size of the simulated final blocks.

The model was more successful on the segmented portion of the mandible, which is both smaller and significantly more rectangular than the complete mandible. Across 100 trials, the model was able to generate a configuration with over 90% connectivity score in all 100 cases, with 98 out of 100 surpassing 95% total connectivity. Figure 7 shows the average and range of connectivity scores for both the whole mandible and mandibular segment. Although both shapes have comparable performance on average, the model occasionally has a worse performance on the mandible, which is the significantly more complicated shape between the two.

In both cases, the final block structure is very similar to the original shape. Figure 8 shows a 3D rendering of both the complete mandible with 7mm blocks and the mandibular segment with 10mm blocks. Both of these 3D models were built directly from the model output. In both cases, the overall shape of the block structure is a good approximation to the original shape despite the block size limiting the details. Together, the stack representation provides build instructions for the shape fit configuration while the 3D model provides a digital preview of the physical structure.

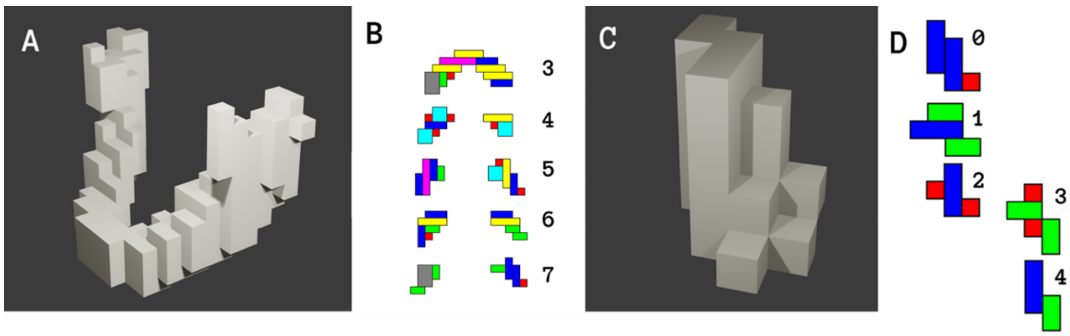

Figure 8. (A) 3D render of the mandible constructed with 7mm blocks. (B) Z-slices 3-7 of the block instructions for building the 3D mandible structure. (C) 3D render of the sagittal cut of the ramus, constructed with 10mm blocks. (D) All Z-slices of the ramus segment showing blocks used to construct the 3D shape.

The model saw a significant drop in performance moving from the smaller ramus segment to the full mandible, both in connectivity and with the required number of blocks for the configuration. While it may be the case that a more advanced model could remedy the deficiencies in constructing a connected shape fit configuration, the block size issue is less easily overcome simply because of the physical constraints. A larger shape will require more blocks by nature, but continually increasing block size is not a universal solution because it will come alongside a decrease in fine detail of the final build.

The experimental results demonstrate that the model can generate good shape fit configurations on clinically relevant data. The primary takeaway from these trials is that the cubic or rectangular blocks are much more limited for highly complex geometries such as the full mandible. This model is more relevant to less extreme bone defects, such as the ramus, and is less suited to applications of complete mandibular reconstruction. Another alternative to consider is the creation of larger, more anatomically correct structures, such as the body of the mandible, which then have additive locations to customize the ends near the ramus with the smaller blocks.

Discussion

The goal for the computational aspects of this collaborative project is to create a clinically viable product using the modular scaffolding system. This current research takes a meaningful step towards that goal by introducing a computational model for automated LEGO model configuration, an important consideration with potential for introduction to the clinical offsetting for this technology which will ease implementation for the surgeons involved.

The computational test results presented demonstrate the early theoretical success of the model in creating stable configurations on a variety of standard and clinical shapes while representing those configurations in a user-readable manner. These results show the proof of concept of the model to assist in clinical implementation for future studies. From the experimental data, we demonstrated the model's ability to generate highly connected configurations for both a complete mandible and an artificial defect created by segmenting a portion of the mandible. However, reconstructing the entire mandible is a much more computationally demanding task compared to the smaller segment. Additionally, due to its complex geometry, accurately reconstructing the mandible required between 148 and 217 blocks across 100 trial configurations. This is far higher than the rough goal of 50 blocks for construction, and to align these two values would require the mandible to be viewed in even lower resolution. While this is possible, over-aggressive downsampling risks erasing crucial structural detail of the mandible and may inhibit proper reconstruction. Due to this constraint, it may be the case that this method of craniomaxillofacial reconstruction is more applicable to smaller defects, rather than complete zygomatic or mandibular reconstruction.

The biggest current limitation is the experimental application, both in terms of building configurations to fit human craniomaxillofacial defects and in terms of understanding how the computational stability of a shape fit configuration translates to physical robustness. Without this application and testing, there is a lack of information on the biomechanical aspect of the shape fit configurations such as expected stress forces and level of fill required for best healing outcomes for patients. Although these can be estimated from finite-element modeling programs and previous research into 3D-printed scaffolding, it remains a strong consideration. However, we are currently making efforts to acquire clinical images to further optimize the model and provide experimental testing and validation.

There are three primary directions for future computational work on this project. The first is to extend the algorithm to consider blocks with varying heights, as these blocks could greatly impact both the number of blocks required to create a shape fit and the overall stability of the final result. Currently, the model assumes blocks of height 1 unit, but that is not necessarily the most effective set of blocks. There has also been discussion of fabricating blocks which are rounded on the top face, designed for the topmost layer of a configuration to reduce the number of sharp edges and corners. Including these additional blocks could improve the fit of the configuration to the original defect and improve bone growth.

The second direction would be to obtain and analyze additional experimental data. This could inform currently arbitrary parameters such as the optimal unit size of the 1x1x1 block (i.e., 4mm, 10mm, etc.) and the most common block shapes. Initial results indicate that longer, skinnier blocks, especially those with dimension 1x1xN, are the most frequently chosen blocks for building configurations, however, this may not necessarily be the case for the majority of craniomaxillofacial defects. It is also currently unknown whether the connected configurations will hold up under mechanical stressors, and it is possible that block dimensions will affect the physical robustness of a configuration. Further work will seek to simulate mechanical loading in finite element analysis models in the Mimics software from the output shapes produced by the models presented here.

Overall, this model provides a starting point for developing shape fit configurations for craniomaxillofacial defects. We have shown that we can algorithmically generate stable, connected shape fit configurations for complex shapes which preserve >95% of the original shape with a variety of potential block dimensions.

Appendix A: Software Specification

FileImport.py

Dependencies: numpy, matplotlib.pyplot, PIL.Image, os, sys, subprocess

Class ImageImport()

import_zstack(self, folder, img_format, binary) -> np.ndarray

scale(arr, iscale, dscale) -> np.ndarray

convert_stack_to_cubes(arr) -> np.ndarray

save_to_zstack_binary(array, outfolder) -> None

save_to_zstack_color(array, outfolder) -> None

save_to_zstack_borders(array, outfolder) -> None

Class ObjImport(ImageImport)

import_obj(self, file, vertex_spacing) -> np.ndarray

import_stl(self, file, vertex_spacing) -> np.ndarray

Graph.py

Dependencies: numpy, logging

Class Edge()

__str__(self) -> str

Class Block()

update_block_label_index() -> None

info(self) -> str

get_area() -> int

find_edges(self, others) -> list[Edge]

merge(self, other) -> Block | None

search(self) -> True

Class Graph()

add_block(self, block) -> None

info(self) -> str

create_edges(self) -> None

recompute_edges(self, level) -> None

as_array(self) -> np.ndarray

as_subgraphs(self) -> np.ndarray

as_colors(self) -> np.ndarray

log(self, folder) -> None

data(self, filename) -> None

block_size_stats(self) -> str

split(self, block_index, level) -> None

is_legal(self, block) -> bool

merge(self, block_index, level) -> bool

search(self, block, subgraph_index, bottom, top) -> None

find_subgraphs(self, bottom, top) -> int

get_largest_subgraph(self) -> dict

Configuration.py

Dependencies: numpy, random, logging, Graph.Graph, Graph.Block, copy.deepcopy

Class CubeConfiguration()

merge(graph, block_index, level_index) -> None select_random_square(input_array, level) -> (int, int, int)

find_largest_block(input, x, y, z, max_block_width, max_block_length) -> Block

construct_randomized_graph(input_array) -> Graph

run_evolution(self, graph) -> None

run_level_evolution(self, graph, level) -> int

refill_level(self, g, z) -> None

fill_level(self, input_array, g, z) -> None

build_configuration(self, input_array) -> Graph

Bibliography

Bertassoni, L. E. (2022). Bioprinting of complex multicellular organs with advanced functionality – recent progress and challenges ahead. *Advanced Materials (Deerfield Beach, Fla.)*, *34*(3), e2101321. https://doi.org/10.1002/adma.202101321

Brennan, J. (2006). Experience of first deployed otolaryngology team in Operation Iraqi Freedom: The changing face of combat injuries. *Otolaryngology--Head and Neck Surgery: Official Journal of American Academy of Otolaryngology-Head and Neck Surgery*, *134*(1), 100–105. https://doi.org/10.1016/j.otohns.2005.10.008

Ho, N., Hollister, S., Agrawal, V., Flanagan, C., Lee, C., Wheeler, M., Wang, H., Ebramzadeh, E., & Sangiorgio, S. (2022). Evaluation of Topology Optimization Using 3D Printing for Bioresorbable Fusion Cages: A Biomechanical Study in A Porcine Model. *Spine*, *Publish Ahead of Print*. https://doi.org/10.1097/BRS.0000000000004491

J Wallner & J Egger. (2018). *Mandibular CT Dataset Collection* [Dataset]. Figshare.

Lee, S., Kim, J., Kim, J. W., & Moon, B.-R. (2015). Finding an Optimal LEGO® Brick Layout of Voxelized 3D Object Using a Genetic Algorithm. *Proceedings of the 2015 Annual Conference on Genetic and Evolutionary Computation*, 1215–1222. https://doi.org/10.1145/2739480.2754667

Lee, S. S., Du, X., Smit, T., Bissacco, E. G., Seiler, D., de Wild, M., & Ferguson, S. J. (2023). 3D-printed LEGO®-inspired titanium scaffolds for patient-specific regenerative medicine. *Biomaterials Advances*, *154*, 213617. https://doi.org/10.1016/j.bioadv.2023.213617

Lopez, M. A., & Arnholt, J. L. (2007). Safety of Definitive In-Theater Repair of Facial Fractures. *Archives of Facial Plastic Surgery*, *9*(6), 400–405. https://doi.org/10.1001/archfaci.9.6.400

Murphy, S. V., De Coppi, P., & Atala, A. (2020). Opportunities and challenges of translational 3D bioprinting. *Nature Biomedical Engineering*, *4*(4), 370–380. https://doi.org/10.1038/s41551-019-0471-7

Neubauer, D. C., Camacho, M., O'Reilly, E. B., Brice, M., Gurney, J. M., & Martin, M. J. (2022). The new face of war: Craniofacial injuries from Operation Inherent Resolve. *The Journal of Trauma and Acute Care Surgery*, *93*(2S Suppl 1), S49–S55. https://doi.org/10.1097/TA.0000000000003700

Pilipchuk, S., Monje, A., Jiao, Y., Hao, J., Kruger, L., Flanagan, C., Hollister, S., & Giannobile, W. (2016). Integration of 3D Printed and Micropatterned Polycaprolactone Scaffolds for Guidance of Oriented Collagenous Tissue Formation In Vivo. *Advanced Healthcare Materials*, *5*. https://doi.org/10.1002/adhm.201500758

Prévost, R., Whiting, E., Lefebvre, S., & Sorkine-Hornung, O. (2013). Make it stand: Balancing shapes for 3D fabrication. *ACM Transactions on Graphics*, *32*(4), 81:1-81:10. https://doi.org/10.1145/2461912.2461957

Smith, B., Kaufman, D. M., Vouga, E., Tamstorf, R., & Grinspun, E. (2012). Reflections on simultaneous impact. *ACM Transactions on Graphics*, *31*(4), 106:1-106:12. https://doi.org/10.1145/2185520.2185602

Stava, O., Vanek, J., Benes, B., Carr, N., & Měch, R. (2012). Stress relief: Improving structural strength of 3D printable objects. *ACM Transactions on Graphics*, *31*(4), 48:1-48:11. https://doi.org/10.1145/2185520.2185544

Subbiah, R., Hipfinger, C., Tahayeri, A., Athirasala, A., Horsophonphong, S., Thrivikraman, G., França, C. M., Cunha, D. A., Mansoorifar, A., Zahariev, A., Jones, J. M., Coelho, P. G., Witek, L., Xie, H., Guldberg, R. E., & Bertassoni, L. E. (2020). 3D Printing of Microgel-Loaded Modular Microcages as Instructive Scaffolds for Tissue Engineering. *Advanced Materials (Deerfield Beach, Fla.)*, *32*(36), e2001736. https://doi.org/10.1002/adma.202001736

Subbiah, R., Lin, E. Y., Athirasala, A., Romanowicz, G. E., Lin, A. S. P., Califano, J. V., Guldberg, R. E., & Bertassoni, L. E. (2023). Engineering of an Osteoinductive and Growth Factor-Free Injectable Bone-Like Microgel for Bone Regeneration. *Advanced Healthcare Materials*, *12*(11), 2200976. https://doi.org/10.1002/adhm.202200976

Thrivikraman, G., Athirasala, A., Gordon, R., Zhang, L., Bergan, R., Keene, D. R., Jones, J. M., Xie, H., Chen, Z., Tao, J., Wingender, B., Gower, L., Ferracane, J. L., & Bertassoni, L. E. (2019). Rapid fabrication of vascularized and innervated cell-laden bone models with biomimetic intrafibrillar collagen mineralization. *Nature Communications*, *10*(1), 3520. https://doi.org/10.1038/s41467-019-11455-8

Umetani, N., Igarashi, T., & Mitra, N. J. (2012). Guided exploration of physically valid shapes for furniture design. *ACM Transactions on Graphics*, *31*(4), 86:1-86:11. https://doi.org/10.1145/2185520.2185582

Valdiri, L. A., Andrews-Arce, V. E., & Seery, J. M. (2015). Training Forward Surgical Teams for Deployment: The US Army Trauma Training Center. *Critical Care Nurse*, *35*(2), e11–e17. https://doi.org/10.4037/ccn2015752

Wallner, J., Hochegger, K., Chen, X., Mischak, I., Reinbacher, K., Pau, M., Zrnc, T., Schwenzer-Zimmerer, K., Zemann, W., Schmalstieg, D., & Egger, J. (2018). Clinical evaluation of semi-automatic open-source algorithmic software segmentation of the mandibular bone: Practical feasibility and assessment of a new course of action. *PLOS ONE*, *13*(5), e0196378. https://doi.org/10.1371/journal.pone.0196378

Willson, K., & Atala, A. (2022). Medical 3D Printing: Tools and Techniques, Today and Tomorrow. *Annual Review of Chemical and Biomolecular Engineering*, *13*, 481–499. https://doi.org/10.1146/annurev-chembioeng-092220-015404

Zopf, D., Mitsak, A., Flanagan, C., Wheeler, M., Green, G., & Hollister, S. (2014). Computer-Aided Designed, 3-Dimensionally Printed Porous Tissue Bioscaffolds For Craniofacial Soft Tissue Reconstruction. *Otolaryngology--Head and Neck Surgery : Official Journal of American Academy of Otolaryngology-Head and Neck Surgery*, *149*. https://doi.org/10.1177/0194599814552065